Catalysis Science & Technology

Accepted Manuscript

ROYAL SOCIETY OF CHEMISTRY

www.rsc.org/catalysis

Journal Name

ARTICLE

Highly Monodisperse Pt(0)@AC NPs as Highly Efficient and Reusable Catalysts: The Effect of the Surfactant on their Catalytic Activities in Room Temperature Dehydrocoupling of DMAB

Received 00th January 20xx,
Accepted 00th January 20xx

DOI: 10.1039/x0xx00000x

www.rsc.org/

Betül Çelik †, Esma Erken †, Sinan Eriş, Yunus Yıldız, Birgütay Şahin, Handan Pamuk, Fatih Sen*

Adressed herein we report the development of highly efficient and monodisperse Pt(0) nanoclusters for the dehydrocoupling of dimethylamine borane (DMAB) which is considered to be one of the new hydrogen storage materials. The prepared Pt(0) nanoclusters were in-situ generated for the first time from the reduction of $PtCl_4$ and using dipentylamine (DPA) and tripentylamine (TPA) ligands on an activated carbon for the dehydrocoupling of dimethylamine-borane at room temperature and characterized by ICP-OES, XRD, TEM, HR-TEM, AFM, EDX, XPS techniques. All results show that highly crystalline and colloidally stable Pt(0)/DPA@AC and Pt(0)/TPA@AC nanoparticles have been formed and Pt(0)/DPA@AC and Pt(0)/TPA@AC were found to be one of the the most active and the long-lived catalysts with superior reusability performance in the dehydrocoupling of DMAB at room temperature.

Introduction

Energy is mostly supplied by the combustion of fossil fuels which emits large amounts of greenhouse gases, thus causes to global warming [1]. On the way towards a sustainable energy future [2], hydrogen appears to be the best energy carrier [3, 4]. However, the safe and efficient storage of hydrogen is still one of the most important and challenging problems in hydrogen economy [5]. For the last decades, there has been rapidly growing interest for searching suitable hydrogen storage materials on the way towards a sustainable energy future [2–5]. Among the various kinds of solid hydrogen storage materials [6–10] dimethyl amine-boranes (DMAB) appears to be one of the most promising solid hydrogen carrier material [11, 12]. DMAB has various advantages like nontoxic, crystalline solid at room temperature, stable in air and water, and environmentally friendly. Of particular interest, recent studies have already showed that DMAB is really a model substrate since the products are relatively easy to understand compared to the other ammonia boranes.

$$2Me_2NHBH_3 \xrightarrow{\text{catalyst}} (Me_2N.BH_2)_2 + 2H_2$$

Scheme 1. The catalytic dehydrocoupling of dimethylamine- borane ($(CH_3)_2NHBH_3$, DMAB).

Further, various homogeneous and heterogeneous catalysts have been tested for dehydrocoupling of DMAB such as Ru, Rh, Pd, and Ir complexes [13], $Ru(H)(PMe_3)(PNP)$ and $trans\text{-}Ru(H)_2(PMe_3)(PNP^H)$ [14], $[Rh(1,5\text{-}cod)(\mu\text{-}Cl)]_2$ [15–17], $[Cp_2Ti]$ [18, 19], $[RuH_2(\eta^2\text{-}H_2)_2(PCy_3)_2]$ and $[RuH2(\eta^2\text{:}\ \eta^2\text{-}H_2B\text{-}N(Me_2)2(PCy_3)_2]$ [20], $RhCl_3$, colloidal Rh/[Oct4N]Cl and Rh/Al_2O_3 [15], laurate-stabilized Rh(0) [21], hexanoate-stabilized Rh(0) [22], aminopropyltriethoxysilane-stabilized Ru(0) [23], Re complexes [24], Rh4-6 clusters [25], $RhCl(PHCy_2)_3$ [26], Ru/ZIF-8 [2], [Ru(p-Cym)(bipy)Cl]Cl [27], Pd(0)/MOF [28], Pt(0)/amylamine [29]. Although the record activity has been achieved by using homogeneous $[\eta^5C_5H_3\text{-}1,3(SiMe_3)_2)_2Ti]_2$ catalyst [30], the current research has focused on the development of new metal nanoparticle catalysts because of their significant advantages in product isolation, catalyst recovery and reusability [29]. We report, for the first time, the preparation and characterization of highly efficient and monodisperse Pt(0) nanoparticles stabilized by dipentylamine (DPA) and tripentylamine (TBA) ligand on an activated carbon, hereafter designated as Pt(0)/DPA@AC and Pt(0)/TPA@AC, respectively. We have also evaluated the effect of the stabilizing ligand on the catalytic activity of room temperature dehydrocoupling of DMAB [$(CH_3)_2NHBH_3$)].

Experimental methods

Reagents and Instrumentation

$PtCl_4$ (99 % Alfa Aesar), tetrahydrofuran (THF) (99.5 %, Merck), lithium triethylborohydride (1.0 M dissolved in THF, Sigma Aldrich), dipentylamine and tripentylamine (Sigma Aldrich), dimethylamine-borane ($(CH_3)_2NHBH_3$) (Sigma Aldrich) were used as received from suppliers. THF was distilled over sodium under argon atmosphere and stored under inert atmosphere. De-ionized water was filtered

Sen Research Group, Biochemistry Department, Faculty of Arts and Science, Dumlupınar University, Evliya Çelebi Campus 43100 Kütahya, Turkey.
† These authors equally contributed to this work.
Electronic Supplementary Information (ESI) available: [details of any supplementary information available should be included here]. See DOI: 10.1039/x0xx00000x

by Millipore water purification system (18 MΩ) analytical grade. All glassware and Teflon-coated magnetic stir bars were cleaned with aqua regia, followed by washing with distilled water before drying.

TEM samples were made ready by dropping of 0.5 mg/mL ethanol solution of the prepared catalysts with an activated carbon support on a carbon covered 400-mesh copper grid, and then the solvent was vaporized. Elimination of excess solution was performed with an adsorbent paper and the sample was dried under vacuum at room temperature before analysis. TEM analysis was carried out by a JEOL 200 kV. More than 300 particles were calculated to get the integrated information about the overall distribution of Pt-based catalyst sample.

During X-ray Photoelectron Spectroscopy (XPS) analysis, Specs spectrometer was employed and as an X-ray source Kα lines of Mg (1253.6 eV, 10 mA) was used. Sample preparation was done by depositing the catalyst on Cu double-sided tape (3M Inc.). C 1s line at 284.6 eV was selected as a reference point and all XPS peaks were fitted using a Gaussian function and the C 1s line at 284.6 eV was used as the reference line.

XRD analysis were performed with a Panalytical Empyrean diffractometer with Ultima+theta–theta high resolution goniometer, having an X-ray generator (Cu K∞ radiation, k = 1.54056 Å) and operating condition of 40 kV and 40 mA.

In order to examine the quantity of platinum in each catalyst, Leeman Lab Inductively Coupled Plazma Spectroscopy (ICP) was occupied.

With the aim of enlightening the surface topographies of the prepared catalysts, AFM technique were used with the sample at ambient temperature using Park Systems AFM XE-100E operated in the intermittent contact ("tapping") mode. We used 0.01-0.025 ohm-cm antimony doped silicon AFM probes (Ultrasharp TESP) having cantilever spring constants of 20−80 N/m and resonance frequencies of 328 - 379 kHz. As an estimation of producer, the tip radius of curvature is approximately 2 nm. For this examination, first, a sample for AFM was prepared by diluting the product solutions by 300-fold or more with DI water and put 2.5 µL of the final solution directly onto the freshly cleaved mica disk (supporting material) and a solvent was dried in a vacuum at room temperature for at least 12 h.

^{11}B NMR spectra were recorded on a Bruker Avance DPX 400 MHz spectrometer (128.2 MHz for ^{11}B NMR).

The in-situ preparation of Pt(0)/DPA@AC and Pt(0)/TPA@AC and their catalytic activities in the dehydrocoupling of DMAB

Prior to beginning the catalytic activity measurements of Pt(0)/DPA@AC and Pt(0)/TPA@AC used in dehydrocoupling of DMAB, a typical jacketed, three-necked reaction flask connected to the water filled cylinder glass tube under a dry nitrogen atmosphere. In order to eliminate existing oxygen and water prior to all catalytic tests, the jacketed reaction flask was kept under vacuum for at least 15 min, and then nitrogen gas was allowed to occupy it. The measurement of the quantity of hydrogen evolution during dehydrocoupling of DMAB was performed so as to examine the catalytic activity of prepared nanoparticles. After the mixing of 0.25 mmol (0.081 g) of $PtCl_4$ dissolved in small amount of anhydrous tetrahydrofuran and 0.25 mmol of DPA or TPA ligand, 1.0 mmol of DMAB in a small amount of THF was added into the jacketed reaction flask thermostatted at 25.0 ± 0.1 ^{o}C, and then hydrogen liberation was started. In order to observe hydrogen gas generation from the catalytic reaction solution, typical water-filled gas burette system was used and water displacement was recorded. After completion of catalytic test, an approximately 0.5 mL aliquot of the reaction solution in the reactor was taken with a glass Pasteur pipet and added to 1 g of $CDCl_3$ in a quartz NMR sample tube.

Reusability performance of Pt(0)/DPA@AC and Pt(0)/TPA@AC in the dehydrocoupling of DMAB

After the first catalytic reaction of the dehydrocoupling of 1.0 mmol of DMAB starting with Pt(0)/DPA@AC and Pt(0)/TPA@AC, reaction flask was disassembled from the line and attached to a vacuum line. After the vaporization of volatiles, the solid residue was weighed and used again in the dehydrocoupling reaction under the same conditions (in a small amount of THF at 25.0 ± 0.1 ^{o}C). This procedure was followed up to four catalytic runs.

Mercury (Hg(0)) poisoning of Pt(0)/DPA@AC and Pt(0)/TPA@AC in the dehydrocoupling of DMAB

Elemental Hg (300 equiv.) was placed into a small amount of THF solution containing Pt(0)/DPA@AC and Pt(0)/TPA@AC in the jacketed, three-necked reaction flask. After 4-hour-stirring, this solution was used in the dehydrocoupling of 1.0 mmol DMAB under the identical situations reported above.

Results and discussion

Characterization of Pt(0)/DPA@AC and Pt(0)/TPA@AC

Easy reproductions of prepared nanoparticles were carried out by in-situ techniques using an anhydrous THF solution of DPA and TPA ligand at room temperature. Without any ligand like DPA and TPA used for stabilization, sudden agglomeration and precipitation out of THF solution of prepared Pt(0) nanoparticles was monitored. This demonstrated that DPA and TPA ligands are highly efficient stabilizing agents for the platinum (0) nanoparticles. Pt(0)/DPA@AC and Pt(0)/TPA@AC were isolated successfully by washing with dry ethanol to eliminate excess ligand and vaporizing the solvent under vacuum atmosphere.

Highly efficient and monodisperse Pt(0)/DPA@AC and Pt(0)/TPA@AC were characterized by ICP-OES, XRD, TEM, HRTEM, AFM and XPS. Spectroscopies and applications of the catalysts were carried out by hydrogen gas production tests for the dehydrocoupling of DMAB.

X-ray diffraction patterns of highly monodisperse Pt(0)/DPA@AC and Pt(0)/TPA@AC are illustrated in Figure 1 and indicate that all diffraction patterns have similar peaks at around 2θ= 39.90, 46.60, 67.50, 81.52, 86.03 and 2θ =39.68, 46.15, 67.32, 81.07, 89.90, respectively**.** These peaks are planes of the face-centered cubic (fcc) crystal lattice of platinum. (JCPDS-ICDD, Card No. 04-802) that is due to Pt (111), (200), (220), (311), and (320) for Pt(0)/DPA@AC and Pt(0)/TPA@AC. In order to find the lattice parameter (αPt) values and average crystallite sizes of the metal particles, the Pt (220)

diffraction peak of the prepared catalysts have been used. The lattice constant values have been calculated to be 3.922 and 3.931 Å for Pt (0)/DPA@AC and Pt(0)/TPA@AC, respectively, which are very close to 3.923 Å obtained by the following equation for pure Pt [31a-e].

$$\sin\theta = \frac{\lambda\sqrt{h^2+k^2+l^2}}{2a}$$ (for a cubic structure)

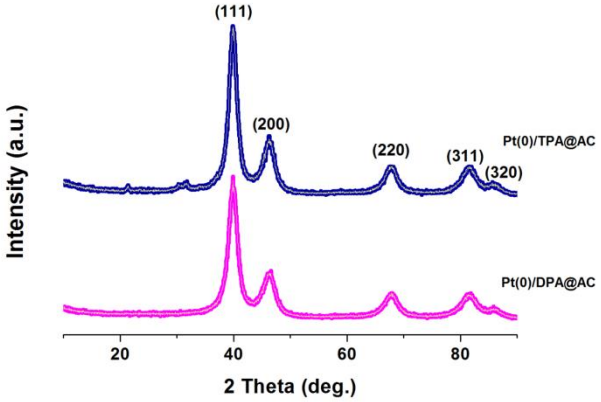

Fig. 1. XRD of Pt(0)/DPA@AC and Pt(0)/TPA@AC

Furthermore, the average crystallite particle sizes of highly monodisperse Pt(0)/DPA@AC and Pt(0)/TPA@AC were calculated to be 3.30± 0.35 nm and 3.77±0.39 nm, respectively by the use of the following formula, [32];

$$d(\text{Å}) = \frac{k\lambda}{\beta\cos\theta}$$

where k= a coefficient (0.9); λ= the wavelength of X-ray used (1.54056 Å), β= the full width half-maximum of respective diffraction peak (rad); θ= the angle at the position of peak maximum (rad).

The high resolution electron micrograph (HRTEM) and particle size histogram of Pt(0)/DPA@AC and Pt(0)/TPA@AC show the highly monodisperse morphology of the catalysts as indicated in Figure 2. The average particle sizes of Pt(0)/DPA@AC and Pt(0)/TPA@AC were found to be 3.48± 0.39 nm and 3.86±0.43 nm and a uniform distribution of the catalyst particles with a very narrow range on activated carbon was detected. The HRTEM results also revealed that most of the particles were in a spherical shape, and no agglomerations were observed in the prepared catalysts. Moreover, the representative atomic lattice fringes obtained by HRTEM for Pt(0)/TPA@AC were shown in Fig 2. and it is found that Pt (111) and (200) plane spacing are 0.228 and 0.196 nm on the prepared catalyst, respectively, which is very close to nominal Pt(111) and (200) spacing of 0.227 and 0.198 nm, respectively [33a-d].

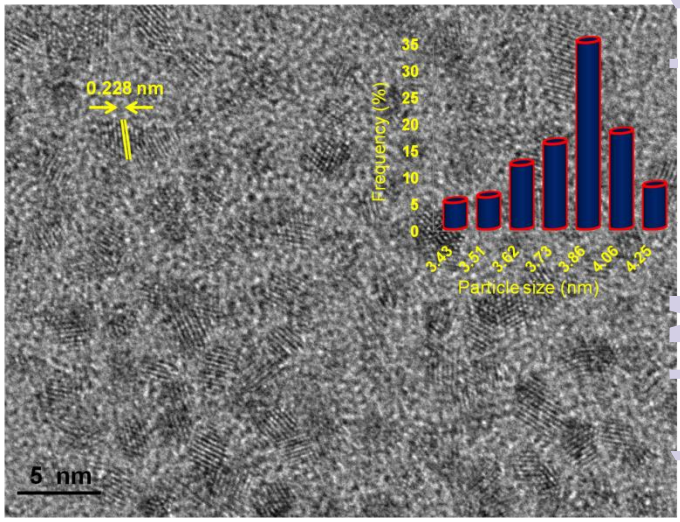

Fig. 2. High resolution transition electron micrograph and particle size histogram of a catalyst Pt(0)/TPA@AC.

The investigation of the height diameter distribution, as shown in Fig. S1, was also carried out by Atomic Force Microscopy (AFM). It was shown that the AFM particle height distributions are very good agreement with the particle size obtained by XRD and TEM.

For determination of the effect of the oxidation state of platinum on catalytic activities for the prepared catalysts, the Pt 4f region has been evaluated by using X-ray photoelectron spectroscopy (XPS). Shirley's method was used to subtract background, then the Gaussian–Lorentzian method was utilized for fitting of all XPS peaks and all peaks were investigated in terms of relative peak area, chemical shifts of Pt. The estimation of the relative intensity of the species was performed by calculating the integral of each peak, after smoothing, subtraction of the Shirley-shaped background. In the XPS spectrum, accurate binding energies (±0.3 eV) were examined by referencing to the C 1s peak at 284.6 eV. It was seen that Pt 4f photoelectron spectrums for the prepared catalysts consist of two pairs of doublet as shown in Fig. 3. For both catalyst, the most intense doublet at about 71.0 and 74.3 eV is the indication of metallic platinum [31a, 32, 34-38] and the other doublet at about 73.9 and 77.4 eV is most probably caused by a very small fraction of oxidized Pt^{4+} species possibly because of unreduced Pt precursor or PtOx species produced during the catalyst in contact with the atmosphere as tabulated in Table 1.

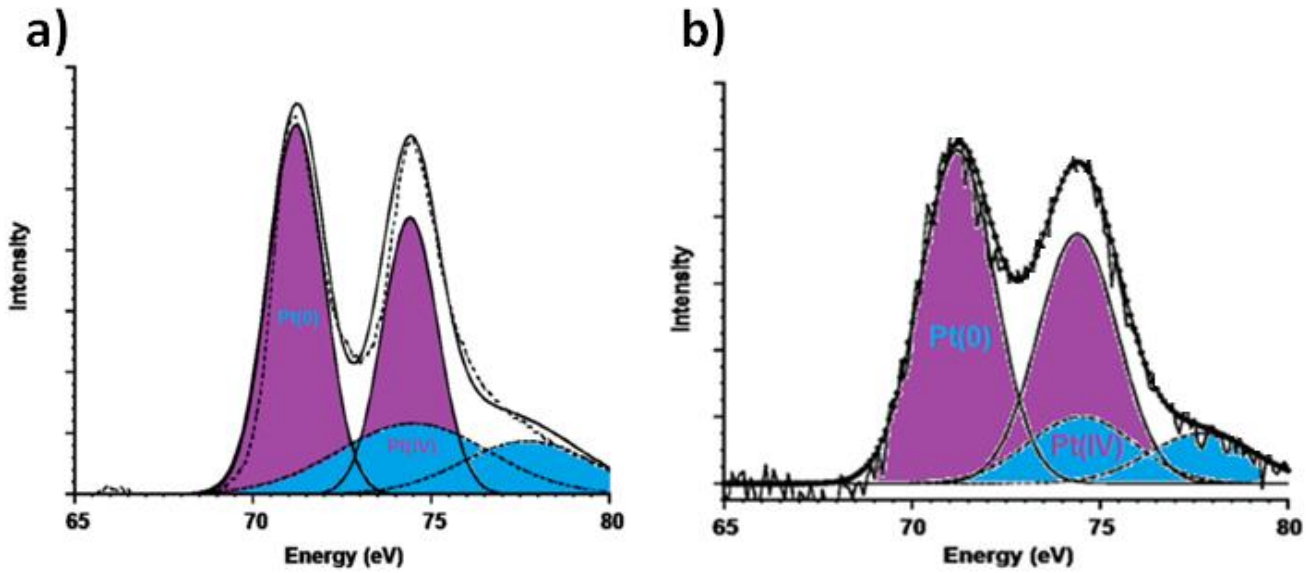

Fig. 3. Pt 4f electron spectra of Pt(0)/DPA@AC (a) and Pt(0)/TPA@AC (b)

Table 1. Pt $4f_{7/2}$ core binding energy, eV, in the prepared catalyst. The number in the parentheses is the relative intensities of the species.

	Pt $4f_{7/2}$	Pt $4f_{7/2}$	
	Pt(0)	**Pt(IV)**	**Pt(0)/Pt(IV)**
Pt(0)/DPA@AC	70.9 (67.0)	73.9 (33.0)	2.03
Pt(0)/TPA@AC	71.0 (74.7)	74.4 (25.3)	2.95

Catalytic activity of Pt(0)/DPA@AC and Pt(0)/TPA@AC in the dehydrocoupling of dimethylamine-borane (DMAB)

In the catalytic dehydrocoupling of DMAB at 25 ± 0.1 °C, Pt(0)/DPA@AC and Pt(0)/TPA@AC was used as catalyst and their catalytic activities were investigated by the measurement of the volume of hydrogen evolution during the reaction and for the determination of the reaction products was carried out by ^{11}B NMR spectroscopy. After the addition of DMAB into a THF solution of Pt(0)/DPA@AC and Pt(0)/TPA@AC, the hydrogen evolution begins quickly with an initial turnover frequency of 32.86 h^{-1} and 34.14 h^{-1} goes on up to 1 equivalent of H_2 per mol DMAB is emitted. It is observed only ~8-10 % conversion after an induction time period (10 min.); when $PtCl_4$ is used as pre-catalyst under the same conditions in the dehydrocoupling of DMAB as shown in Fig. S2. At the end of the reaction, the combination of Pt nanoparticles and their precipitation out of solution were observed within 10 min. by naked eye due to the weakly coordinating chloride anion of $PtCl_4$ which cannot yield enough stabilization for the platinum (0) nanoparticles [39]. NMR data proves the complete conversion of $(CH_3)_2NHBH_3$ (δ= ~12.7 ppm) to $[(CH_3)_2NBH_2]_2$ (δ= ~5 ppm) which shows the dehydrocoupling reaction of DMAB (at 1.0 equiv. H_2 generation) even at room temperature. In addition, in order to identify the heterogeneous nature of Pt(0)/DPA@AC and Pt(0)/TPA@AC in the dehydrocoupling of DMAB, the mercury poisoning experiment was performed and the result shows that the reaction is completely eased after the addition of 300 equiv. of Hg(0) per Pt, that Pt(0)/DPA@AC and Pt(0)/TPA@AC act as heterogeneous catalysts.

Determination of activation parameters (Ea, ΔH#, and ΔS#) for Pt(0)/DPA@AC and Pt(0)/TPA@AC catalyzed dehydrocoupling of DMAB

The stoichiometric ratio of generated H_2 to $(CH_3)_2NHBH_3$ versus time was plotted for the catalytic dehydrocoupling of DMAB starting with highly monodisperse Pt(0)/DPA@AC and Pt(0)/TPA@AC at four different temperatures as shown in Fig. 4. It was monitored that the catalytic dehydrocoupling rate of DMAB was temperature depended.

Additionally, even at low temperature (20 °C), the dehydrocoupling of DMAB can be catalysed by Pt(0)/DPA@AC and Pt(0)/TPA@AC, producing 1.0 equiv. of H_2. The rate constants (k_{obs}) of hydrogen generation from the dehydrocoupling of DMAB were calculated from the linear portions of the plots given in Fig. 5 at four different temperatures in the range of 20–35 °C and were used for the calculation of activation energy, activation enthalpy and activation entropy from the Arrhenius [40] and Eyring [41] plot (Table 2).

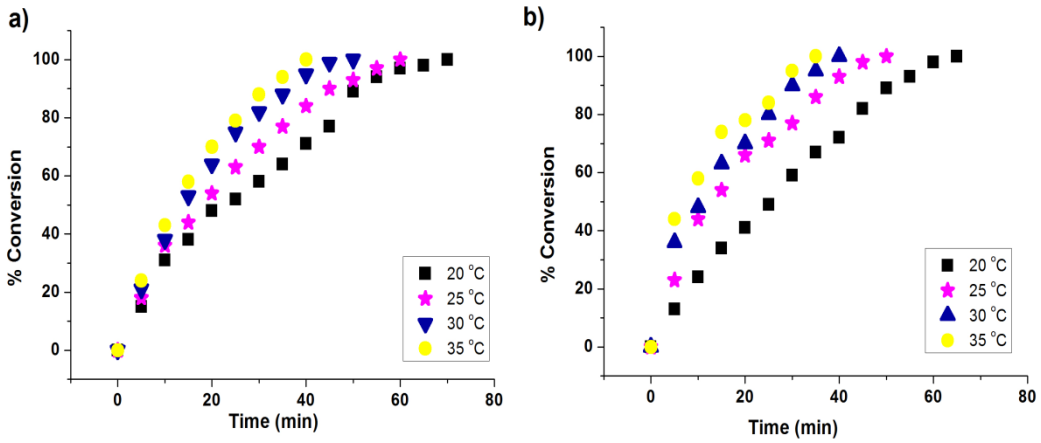

Fig.4. % conversion versus time graph for Pt(0)/DPA@AC (a) and Pt(0)/TPA@AC (b) (7.5% mol) catalysed dehydrocoupling of DMAB in THF at various temperatures as given on the graph Pt(0)/DPA@AC and Pt(0)/TPA@AC

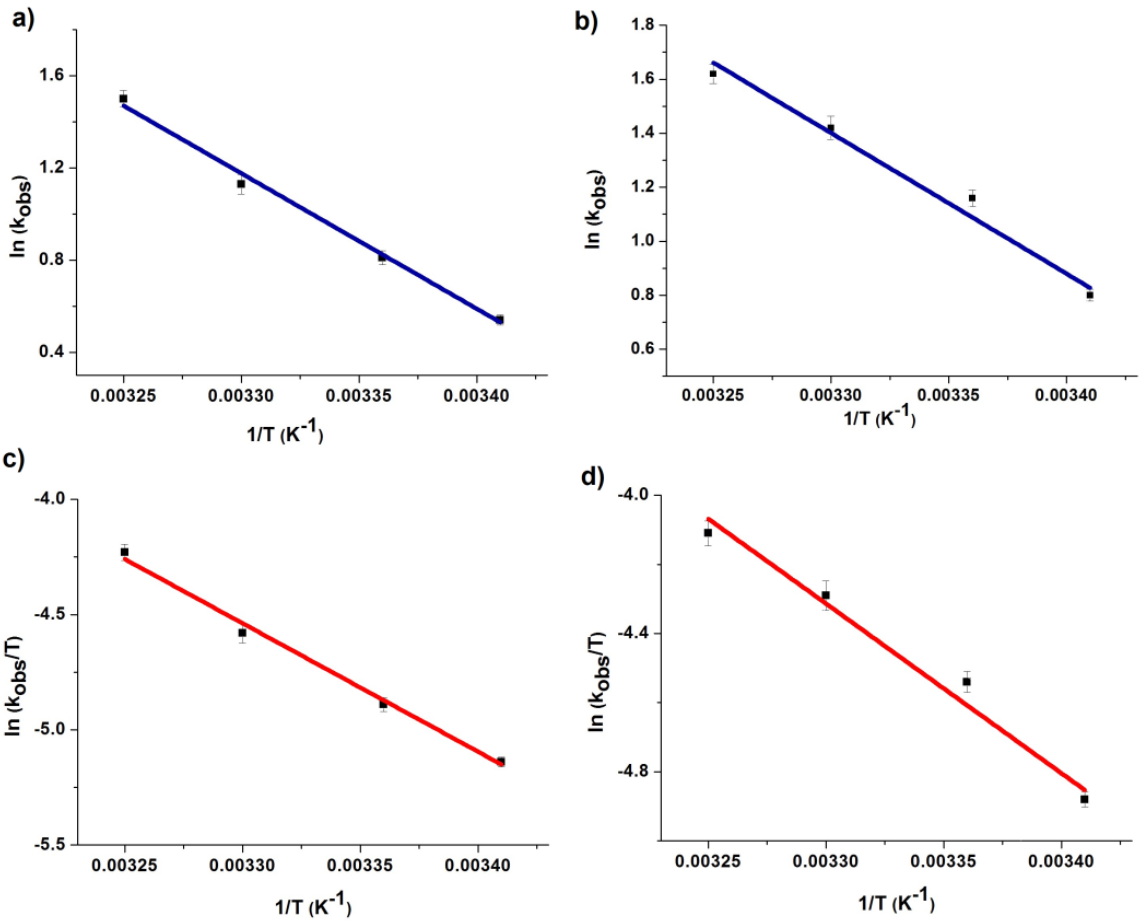

Fig. 5. (a,b) Arrhenius and (c,d) Eyring plots for Pt(0)/DPA@AC (a,c) and Pt(0)/TPA@AC (b,d) catalysed dehydrocoupling of DMAB at various temperatures

Table 2. The activation energy (Ea), activation enthalpy ($\Delta H^{\#}$), and activation entropy ($\Delta S^{\#}$) values from the Arrhenius and Eyring plots for Pt(0)/DPA@AC and Pt(0)/TPA@AC

	Ea (kJ mol^{-1})	$\Delta H^{\#}$(kJ mol^{-1})	$\Delta S^{\#}$(J mol^{-1} K^{-1})
Pt(0)/DPA@AC	**48.83**	**46.31**	**-115.09**
Pt(0)/TPA@AC	**43.31**	**40.79**	**-98.75**

The activation energy values (43.31 kJ mol-1 for Pt(0)/TPA@AC and 48.83 kJ mol-1 for Pt(0)/DPA@AC) obtained by highly monodisperse Pt(0)/DPA@AC and Pt(0)/TPA@AC are not only higher than Rh(0) nanoparticles (34 kJ mol mol^{-1}), but also still smaller than the activation energy written in the literature for the same reaction as tabulated in Table 3. It can be concluded that highly monodisperse Pt(0)/DPA@AC and Pt(0)/TPA@AC have performed one of the highest catalytic activities for the dehydrocoupling of DMAB reaction. Moreover, it is understood that there is an associative mechanism in the transition state for the catalytic dehydrocoupling of DMAB between the higher negative value of the activation entropy and the small value of the activation enthalpy**.** Furthermore, the data indicate that Pt(0)/TPA@AC, which is stabilized by the more branched ligand, TPA, has increased the catalytic activity compared to Pt(0)/DPA@AC most probably due to higher Pt(0) to Pt(IV) ratio. Furthermore, since the excess of more branched surfactant, TPA, on catalyst can easily be removed from Pt(0)/TPA@AC compared to the Pt(0)/DPA@AC, which creates a more active surface area for the dehydrocoupling of DMAB reactions, the catalytic activity of Pt(0)/TPA@AC is higher than that of Pt(0)/DPA@AC.

It has been found that the structure of surfactant has an effect on the final size of metal nanoparticles; for example, the average particle size of Pt(0)/TPA@AC is larger than that of Pt(0)/DPA@AC. It can be explained that an increase in the particle size might be due to the more branched structure of the TPA compared to the DPA ligand. A more branched surfactant may have a tendency to form a larger hole in the micelles, which in turn would cause an increase in the particle size of the metal which forms in the cavity of the micelle that was confirmed by AFM, XRD crystallite size, and TEM results.

Reusability performance of Pt(0)/DPA@AC and Pt(0)/TPA@AC in the catalytic dehydrocoupling of DMAB

Pt(0)/DPA@AC and Pt(0)/TPA@AC were also examined in order to find whether the prepared catalyst isolable and reusable in the dehydrocoupling of DMAB at room temperature. After the completion of dehydrocoupling of DMAB, highly monodisperse Pt(0)/DPA@AC and Pt(0)/TPA@AC were isolated as black powder, dried in a vacuum and then bottled under N_2 atmosphere. The removed catalysts were observed to be still active in the dehydrocoupling of DMAB. Even if at the fourth catalytic run, they maintain >80 of their initial activity (see Fig. S3). This demonstrates that the prepared platinum nanoparticles are isolable, bottleable, and redispersible yet catalytically active. That is, they can catalyse the dehydrocoupling of DMAB actively several times. The precipitation of bulk Pt(0) metal may cause the slight decline in catalytic activity in following turns. This condition can be seen at the end of the 4^{th} catalytic run, at the end forming a clear, colorless (i.e.,Pt(0) nanoparticle free) by increasing boron products, which blocks the active sites.

In fact, the P-XRD pattern of the sample after the 4^{th} catalytic performance reveals that Pt(0) nanoparticles starts to agglomerate [42]. It is obvious that the initial TOF value of Pt(0)/TPA@AC (34.14 h^{-1}) is higher than the majority of those of other heterogeneous and homogeneous catalysts listed in (see Table 3), except for the prior best heterogeneous (60 h^{-1})[22] and homogeneous [30] (420 h^{-1}) catalysts. Except for the Ru(0)/APTS [23], it is understood that our catalyst is the second best catalyst example of an isolable and reusable nanocatalyst utilized in this substantial catalytic reaction. Most significantly, the reusability performance of our new Pt(0) nanocatalysts is also much better than the previously known most active Rh(0) nanocatalysts which does not have enough stability for isolability and reusability, due to adequate stability of DPA and TPA in our catalyst system, except Rh (0) nanoparticles.

Table 3. Catalysts tested in the dehydrocoupling of DMAB under mild conditions (≤25 °C)

Entry	(Pre) Catalysts	Cov. (%)	TOF	Ref
1	$[RuH(PMe_3)(NC_2H_4PPr_2)_2]$	100	1.5	14
2	$[(C_5H_3\text{-}1,3(SiMe_3)_2)_2Ti]_2$	100	420.0	30
3	$[Rh(1,5\text{-}cod)(dmpe)]PF_6$	95	1.7	13
4	$[Cr(CO)_5(\eta^1\text{-}BH_3NMe_3)]$	97	19.9	43
5	*trans*-$PdCl_2(P(o\text{-}tolyl)_3)_2$	20	0.2	13
6	*trans*-$RuMe_2(PMe_3)_4$	100	12.4	13
7	$[Cp^*Rh(m\text{-}Cl)Cl]_2$	100	0.9	13
8	Ru(0)/APTS	100	55.0	23
9	(Idipp)CuCl	100	0.3	44
10	Ni(skeletal)	100	3.2	45
11	Rh(0)NPs	100	60.0	22
12	Pt(0)/DPA@AC	100	32.86	This study
13	Pt(0)/TPA@AC	100	34.14	This study
14	Ru(cod)(cot)	40	1.6	23
15	$RuCl_3.3H_2O$	77	2.7	23
16	$[Ru(1,5\text{-}cod)Cl_2]n$	70	2.5	23
17	$[Rh(1,5\text{-}cod)_2]Otf$	95	12.0	13
18	$HRh(CO)(PPh_3)_3$	5	0.1	13
19	$[Ir(1,5\text{-}cod)\ \mu\text{-}Cl]_2$	95	0.7	13
20	$RhCl(PPh_3)_3$	100	4.3	13
21	$Rh(0)/[Noct_4]Cl$	90	8.2	13
22	$[RhCl(PHCy_2)_3]$	100	2.6	26
23	$[Rh(1,5\text{-}cod)\ \mu\text{-}Cl]_2$	100	12.5	13
24	$RhCl_3$	90	7.9	13
25	Cp_2Ti	100	12.3	18
26	$[Cr(CO)_5(thf)]$	97	13.4	43
27	Pd/C	95	2.8	13
28	$IrCl_3$	25	0.3	13
29	Pt(0)/BA	100	24.88	46
30	Pt(0)/TBA	100	31.24	46

Conclusions

In conclusion, Pt(0)/DPA@AC and Pt(0)/TPA@AC reproducibly prepared by the in-situ optimized reduction method during the catalytic dehydrocoupling of DMAB at room temperature. The characterization of this highly efficient catalysts by using ICP-MS, P-XRD, XPS, TEM, HRTEM and NMR spectroscopies reveals the formation of highly monodisperse Pt(0) nanoparticles. The catalytic performances of both Pt(0)/DPA@AC and Pt(0)/TPA@AC in terms of activity, life-time and reusability performances was investigated for the catalytic dehydrocoupling of dimethylamine-borane in THF at room temperature. Pt(0)/DPA@AC and Pt(0)/TPA@AC showed unprecedented catalytic activities among all the heterogeneous catalysts tested in the dehydrocoupling of DMAB at room temperature providing an initial TOF value of 32.86 h^{-1} and 34.14 h^{-1} at complete conversion of DMAB to cyclic diborazane ($[Me_2NBH_2]_2$) and generation of 1 equiv.of H_2 per mole of DMAB, respectively. Pt(0)/DPA@AC and Pt(0)/TPA@AC were also found to be highly stable against agglomeration and leaching throughout the catalytic runs in the dehydrocoupling of DMAB, which make them highly reusable and long-lived catalyst. Those catalysts retain

almost their inherent catalytic activity (80%) even at the forth catalytic reuse in hydrogen releasing from dimethylamine-borane. It has been also found that the structure of surfactant has an effect on the final size and correspondingly catalytic activities of metal nanoparticles. The average particle size of Pt(0)/TPA@AC is larger than that of Pt(0)/DPA@AC most probably due to the more branched structure of the TPA compared to the DPA ligand. A more branched surfactant may have a tendency to form a larger hole in the micelles, which in turn would cause an increase in the particle size of the metal which forms in the cavity of the micelle that was confirmed by AFM, XRD crystallite size, and TEM results. Furthermore, the catalytic activity of Pt(0)/TPA@AC is higher than that of Pt(0)/DPA@AC likely owing to easily isolation of the excess of more branched surfactant, TPA, on catalyst compared to the other, which creates a more active surface area for the dehydrocoupling of DMAB reactions,

Understanding the existing synergistic effects between the metal and DPA, TPA ligand remains an active area of research in our group. High catalytic activity, reusability and simple preparation and isolation procedures make Pt(0)/DPA@AC and Pt(0)/TPA@AC very attractive catalyst for performing selective dehydrocoupling reactions.

Acknowledgements

The authors would like to thank to Dumlupinar University BAP (2015-50) for the financial support. The partial support by Science Academy is gratefully acknowledged.

Notes and references

1 Basic Research Needs For the Hydrogen Economy, Report of the Basic Energy Sciences Workshop on Hydrogen Production, Storage and Use, May 13–15, **2003**, Office of Science, U. S. Department of Energy.
2 Gulcan, M.; Zahmakiran, M.; Özkar, S. *Appl. Catalysis B: Environmental* **2014**, *147*, 394– 401.
3 Annual Energy Outlook 2005 With Projections To 2025, Energy Information Administration, February **2005**.
4 Turner, J.; Sverdrup, G.; Mann, K.; Maness, P. G.; Kroposki, B.; Ghirardi, M.; Evans, R. J.; Blake, D. *Int. J. Energy Res.* **2007**, *32*, 379.
5 IAC Report, Lighting the Way Towards a Sustainable Energy Futures, Interacademy Council, Amsterdam, **2007**.
6 Grochala, W.; Edwards, P. P. *Chem. Rev.* **2004**, *104*, 1283.
7 Chen, P.; Xiong, Z. T.; Luo, J. Z.; Lin, J. Y.; Tan, K. L. *Nature* **2002**, *420*, 302.
8 Bacsa, R.; Laurent, C.; Morishima, R.; Suzuki, H.; Lelay, M. *J. Phys. Chem. B* **2004**, *108*, 12718.
9 Lim, S. H.; Luo, J.; Zhong, Z.; Ji, W.; Lin, J. *Inorg. Chem.* **2005**, *44*, 4124.
10 Rood, J. A.; Noll, B. C.; Henderson, K. W. *Inorg. Chem.* **2006**, *45*, 5521.
11 Basic Research Needs Catalysis for Energy, Report from the US Department of Energy, Basic Energy Sciences Workshop Report, August 6–8, **2007**.
12 Wang, J.; Wasmus, S.; Savinell, R. F. *J. Electrochem. Soc.* **1995**, *142*, 4218.
13 Jaska, C.A.; Temple, K.; Lough, A.J.; Manners, I. *J. Am. Chem. Soc*. **2003**, *125*, 9424–9434.
14 Friederich, A.; Drees, M.; Schneider, S. *Chem*. *Eur. J*. **2009**, *15*, 10339–10342.
15 Jaska, C.A.; Manners, I. *J. Am*. *Chem*. *Soc*. **2004**, *126*, 9776–9785.
16 Chen, Y.; Fulton, J.L.; Linehan, J.C.; Autrey, T. *Prepr. Pap. Am. Chem. Soc. Div. Fuel Chem.* **2004**, *49*, 972–973.
17 Chen, Y.; Fulton, J.L.; Linehan, J.C.; Autrey, T. *J. Am*. *Chem*. *Soc*. **2005**, *127*, 3254–3255.
18 Clark, T.J.; Russell, C.A.; Manners, I. *J. Am*. *Chem*. *Soc*. **2006**, *128*, 9582–9583.
19 Sloan, M.E.; Staubitz, A.; Clark, T.J.; Russell, C.A.; Lloyd-Jones, G.C.; Manners, I. *J. Am*. *Chem*. *Soc*. **2010**, *132*, 3831–3841.
20 Alcaraz, G.; Vendier, L.; Clot, E.; Sabo-Etienne, S. *Angew*. *Chem*. *Int*. *Ed*. **2010**, *49*, 918–920.
21 Durap, F.; Zahmakıran, M.; Özkar, S. *Appl*. *Cat*. *A Gen.* **2009**, *369*, 53–59.
22 Zahmakıran, M.; Özkar, S. *Inorg*. *Chem*. **2009**, *48*, 8955–8964.
23 Zahmakıran, M.; Tristany, M.; Philippot, K.; Fajerweg, K.; Özkar, S.; Chaudret, B.*Chem*. *Commun*. **2010**, *46*, 2938–2940.
24 Jiang, Y.; Berke, H. *Chem*. *Commun*. **2007**, *34*, 3571–3573.
25 Fulton, J.L.; Linehan, J.C.; Autrey, T.; Balasubramanian, M.; Chen, Y.; Szymczak, N.K. *J. Am*. *Chem*. *Soc*. **2007**, *129*, 11936–11949.
26 Sloan, M.E.; Clark, T.J.; Manners, I. *Inorg*. *Chem*. **2009**, *48*, 2429–2435.
27 Yurderi, M.; Bulut, A.; Zahmakiran, M.; Gulcan, M.; Özkar, S. *Appl*. *Catal*. *B Environ*. **2014**, *160–161*, 534–541.
28 Munoz-Olasagasti, M.; Telleria, A.; Perez-Miqueo, J.; Garralda, M.A.; Freixa, Z. A . *Dalton Trans*. **2014**, *43*, 11404–11409.
29 Sen, F.; Karatas, Y.; Gulcan, M.; Zahmakiran, M. *RSC Adv.* **2014**, *4*, 1526–1531.
30 Pun, D.; Lobkovsky, E.; Chirik, P.J. *Chem. Commun.* **2007**, *44*, 3297.
31 (a) Liu, Z.; Ling, X.Y.; Su, X.; Lee, J.Y. *J. Phys. Chem. B* **2004,** *108*, 8234-8240. (b) Sen, F.; Sen S.; Gökağaç, G. *Phys. Chem. Chem. Phys.* **2011**, *13*, 1676. (c) Sen, F.; Gökağaç, G. *J. Appl. Electrochem.* **2014**, *44*, 199. (d) Sen, S.; Sen, F.; Gökağaç, G. *Phys. Chem. Chem. Phys.* **2011**, *13*, 6784. (e) Sen, F.; Gökağaç, G. *J. Phys. Chem. C* **2007**, *111*, 1467.
32 H. Klug, L. Alexander, X-ray diffraction procedures, first ed., Wiley, New York, **1954**.
33 (a) Yonezawa, T.; Toshima, N.; Wakai, C.; Nakahara, M.; Nishinaka, M.; Tominaga, T.; Nomura, H. *Coll. and Surf. A* **2000**, *169*, 35-45. (b) Pamuk, H.; Aday, B.; Şen, F.; Kaya, M. *RSC Adv.* **2015**, *5*, 49295. (c) Şen, F.; Gökağaç, G. *Energy & Fuels* **2008**, *22*, 1858–1864. (d) Ozturk, Z.; Sen, F.; Sen, S.; Gokagac, G. *J. Mater. Sci.* **2012**, *47*, 8134–8144.
34 Sen, F.; Gökağaç, G. *J. Phys. Chem. C* **2007,** *111*, 5715-5720.
35 Sumodjo, P.T.A.; Silva, E.J.; Rabochai, T. *J. Electroanal. Chem.* **1989,** *271*, 305.
36 Ertan, S.; Sen, F.; Sen, S.; Gökağaç, G. *J. Nanopart. Res.* **2012**, *14*, 922.
37 Sen, F.; Gökağaç, G.; Sen, S. *J. Nanopart. Res.* **2013**, *15*, 1979.
38 Deivaraj, T.C.; Chen, W.X.; Lee, J.Y. *J. Mater. Chem.* **2003**, *13,* 2555.
39 Özkar, S.; Finke, R. G. *J. Am. Chem. Soc.* **2002**, *124*, 5796.
40 Laidler KJ. Chemical Kinetics. 3rd edn. Benjamin-Cummings: UK; **1997**.
41 Eyring, H. *J. Chem. Phys.* **1935**, *3*, 107.
42 Sun, Y.; Zhuang, L.; Lu, J.; Hong,X.; Liu, P. *J. Am. Chem. Soc.* **2007,** *129,* 15465.
43 Kawano, Y.; Uruichi, M.; Shiomi, M.; Taki, S.; Kawaguchi, T.; Kakizawa, T.; Ogino, H. *J. Am. Chem. Soc.* **2009**, *131*, 14946.
44 Keaton, R. J.; Blacquiere, J. M.; Baker, R. T. *J. Am. Chem. Soc.* **2007**, *129*, 11936.
45 Robertson, A. P. M.; Suter, R.; Chabanne, L.; Whittel, G. R.; Manners, I. *Inorg. Chem.* **2011**, *50*, 12680.
46 Erken, E.; Pamuk, H.; Karatepe, Ö.; Başkaya, G.; Sert, H.; Kalfa, O. M.; Şen, F. *J. Clust. Sci.* **2015**, DOI 10.1007/s10876-015-0892-8.

Graphical Abstract

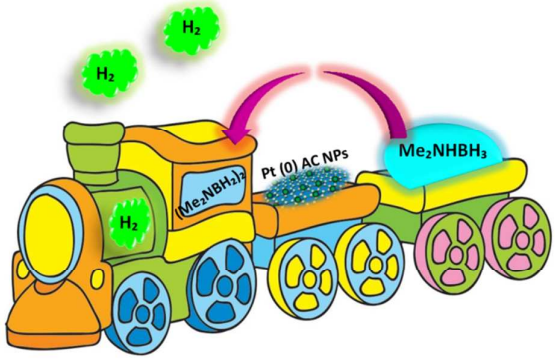

The effect of particle size and the stabilizing ligand on the catalytic activity has been performed for dehydrocoupling of DMAB [$(CH_3)_2NHBH_3$)].